Plasmonic enhancement of photoacoustic strain-waves on gold gratings

De Haan, G.; Abram, E.; Van Den Hooven, T.J.; Planken, P.C.M.

DOI
10.1063/5.0070630

Publication date
2022

Document Version
Final published version

Published in
AIP advances

License
CC BY

AIP Advances

Plasmonic enhancement of photoacoustic strain-waves on gold gratings

Cite as: AIP Advances **12**, 025227 (2022); https://doi.org/10.1063/5.0070630
Submitted: 15 September 2021 • Accepted: 27 January 2022 • Published Online: 23 February 2022

G. de Haan, E. Abram, T. J. van den Hooven, et al.

Plasmonic enhancement of photoacoustic strain-waves on gold gratings

Cite as: AIP Advances 12, 025227 (2022); doi: 10.1063/5.0070630
Submitted: 15 September 2021 • Accepted: 27 January 2022 •
Published Online: 23 February 2022

G. de Haan,[1,2,a] E. Abram,[1,2] T. J. van den Hooven,[1,2] and P. C. M. Planken[1,2]

AFFILIATIONS

[1] Advanced Research Center for Nanolithography (ARCNL), Science Park 106, 1098 XG Amsterdam, The Netherlands
[2] Van der Waals-Zeeman Institute, University of Amsterdam, Science Park 904, 1098 XH Amsterdam, The Netherlands

[a] **Author to whom correspondence should be addressed:** g.dehaan@arcnl.nl

ABSTRACT

In this paper, we report on the time-dependent strain-wave-induced changes in the reflection and diffraction of a gold plasmonic grating. We demonstrate efficient excitation of strain waves using enhanced absorption at and around the surface plasmon polariton resonance. In addition, we observe that the strain-wave-induced changes in the reflection and diffraction of the grating show an approximately quadratic dependence on pump fluence when probed at a wavelength of 400 nm. We tentatively attribute this non-linear behavior to strain-induced nonlinear changes of the interband transition energy. Using a model that calculates the permittivity of the gold taking into account the d to s/p interband transition, we deduce that the interband transition energy would have to change by about 0.013 eV to account for the measured changes in reflection.

I. INTRODUCTION

The ability of ultrafast lasers to generate strain waves in thin metal layers has been investigated extensively in the past.[1–3] Compared to light, the advantage of laser-induced strain waves is that they can travel through optically opaque materials, giving access to a multitude of material properties and physical phenomena.[4–22] Laser-induced strain waves find applications in many fields, such as the detection of buried structures[23–27] and photo-acoustic imaging.[28,29] They also show promise for applications in the semiconductor manufacturing industry for wafer alignment. The presence of strain waves can be detected by measuring changes in the optical properties of the material or by measuring the physical displacement of surfaces and interfaces caused by these waves. Changes in the optical properties can be extracted by either measuring reflection and transmission changes[2] or by measuring diffraction.[18,30] Generally speaking, strain-wave-induced optical changes are small. Therefore, there is a clear need to enhance the optical response to laser-induced strain waves.

In a previous study, we showed that the detection of laser-induced strain waves can be enhanced by probing the effect that they have on a surface plasmon polariton (SPP) resonance.[31] In this way, we were able to show optical signal enhancements of up to a factor of 20 in response to a strain wave. Improving the optical signal strength is important for applications, as this decreases the time needed to obtain a good signal-to-noise ratio. It is interesting to realize that, in principle, an SPP resonance can also be used to increase the amplitude of the strain wave itself in the generation process. This is possible because SPP excitation is accompanied by significantly stronger optical absorption. This would allow for the generation of stronger strain waves at wavelengths where flat metals normally do not absorb much light, i.e., in the near-infrared and infrared region of the spectrum. It would also provide more flexibility in the choice of the wavelength of the light source used for the strain wave generation and/or lower the power requirements for the light source.

Here, we show how grating-coupled SPPs can be used to efficiently *excite* strain waves on gold gratings. In our experiments, we excite SPPs on a gold grating with a period of 440 nm and an amplitude of 47 nm using ultrashort laser pulses with central wavelengths around the SPP resonance at 650 nm. The pump pulses generate several types of strain waves that are detected by

measuring the strain-wave induced reflection and diffraction changes of a synchronized probe pulse with a central wavelength of 400 nm. We find that the pump-induced reflection and diffraction changes reach fairly large values of nearly half a percent, significantly more than what can be achieved on a flat metal surface using transient-grating excitation.[32] Surprisingly, when probing at a wavelength of 400 nm, we find that the strain-wave-induced optical changes scale roughly quadratically with the incident pump fluence, where a linear relation is expected. We tentatively attribute this to non-linear changes of the interband transition energy via strain-induced changes to the band structure of the gold. Our results show that SPPs can be used to more efficiently excite strain waves on structured metal surfaces.

II. EXPERIMENTAL SETUP

A schematic drawing of the experimental geometry is given in Fig. 1. A more detailed explanation and drawing of the entire setup can be found in Ref. 31. In short, the output of an amplified Ti:sapphire laser (Astrella, Coherent) with a repetition rate of 1 kHz, a central wavelength of 800 nm, a pulse length of 35 fs, and an average power of 6 W is split into two using an 85/15 beamsplitter. The stronger beam (pump beam) travels through a three-stage optical parametric amplifier (OPA, HE-TOPAS, from LightConversion). The OPA generates tunable infrared laser pulses with central wavelengths ranging from 1200 to 1400 nm with a maximum pulse energy of about 1 mJ. Afterward, the beam is frequency-doubled using a β-Barium Borate (BBO) crystal generating pulses with a central wavelength tunable from 600 to 700 nm. The beam passes through a mechanical chopper that is synchronized with the 1 kHz pulse train from the laser. With a 50% duty-cycle, the chopper reduces the repetition rate of the pump to 500 Hz, so that every other pump pulse is blocked. Finally, the beam is focused onto the sample to a spot with a diameter of 600 μm. The pump beam illuminates the sample under an angle of ~21° such that the SPP resonance is located at 650 nm.

The weaker beam (probe beam) passes through a variable optical delay line after which it is frequency-doubled, using another BBO crystal, to a central wavelength of 400 nm. The beam is then focused onto the grating under a five-degree angle of incidence to a spot with a diameter of about 300 μm. The polarization of the electric field of the probe beam is perpendicular to the grating lines. The reflection and diffraction of the probe beam are measured using silicon photodiodes. In an unperturbed state, the grating reflects and diffracts 18% and 11% of the probe beam, respectively.

The two samples used in the experiments are made by thermally evaporating 139 nm (117 nm) of gold on top of a commercially available SiO_x grating on a Si substrate (NanoPHAB B.V.). To fabricate the SiO_x grating, 200 nm of SiO_x is deposited on top of a Si substrate. Afterward, the grating is printed onto the SiO_x by electron beam lithography, and the exposed part is etched using reactive-ion etching. An atomic force microscopy (AFM) image of one of the samples, after gold deposition, is shown in Fig. 1. Furthermore, a schematic cross section of this sample is shown on the right hand side of Fig. 1. After deposition, the Au layer thickness for this sample is 139 nm. The duty cycle, pitch, and amplitude of the gold grating have been measured to be 71%, 440, and 47 nm, respectively, using AFM measurements. For both samples, white-light reflection experiments clearly show the presence of a plasmonic resonance whose central wavelength shifts with the angle of incidence, as expected. In the experiments, the angle of incidence is experimentally adjusted for maximum absorption at the plasmonic resonance, and the central wavelength and spectrum of the pulses are measured using a fiber-coupled spectrometer.

III. RESULTS AND DISCUSSION

For all pump-probe measurements discussed below, the beam diameters at the surface of the sample of both pump and probe were kept constant with a full width at half maximum (FWHM) beam diameter of 600 and 300 μm, respectively. The probe pulse fluence was kept constant at a relatively low fluence of 2.8×10^{-4} J/cm^2.

A. Pump-induced probe reflection changes

In Fig. 2, we show the pump fluence dependence of the measured reflection changes from the probe beam with polarization

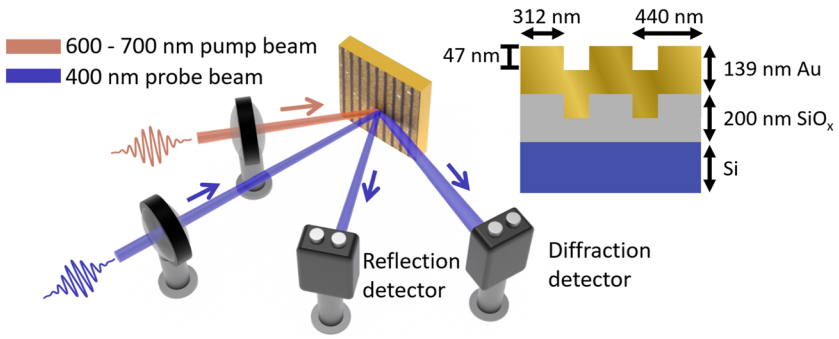

FIG. 1. Schematic drawing of the experimental geometry. The 500 Hz repetition rate, tunable 600–700 nm central wavelength pump pulses illuminate the sample under an angle of 21°, such that they excite the SPP resonance at 650 nm. The 1 kHz repetition rate, 400 nm central wavelength time-delayed probe pulses illuminate the sample under an angle of incidence of five degrees. Both the reflection and diffraction changes of the probe pulse are measured as a function of the time delay between the pump and probe pulses. Projected onto the sample, we show an AFM image of the gold grating. On the right side of the figure, we show a schematic cross section of the sample with all relevant parameters.

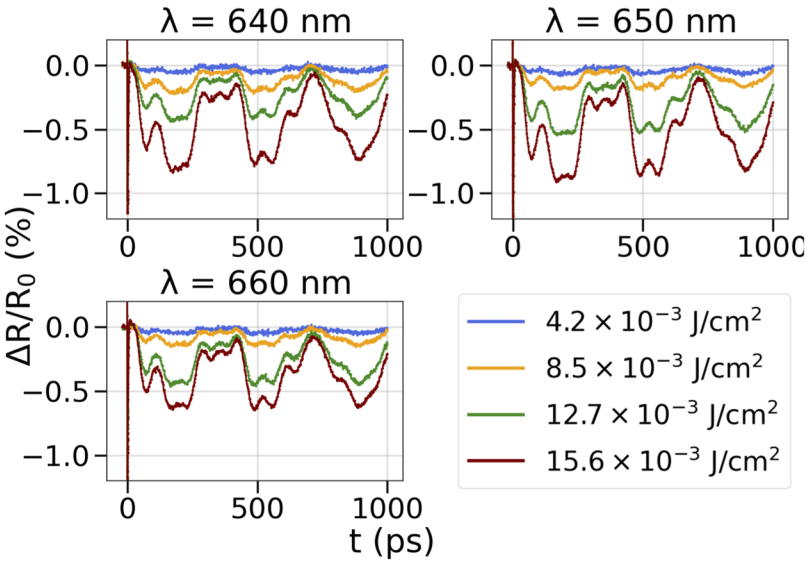

FIG. 2. Pump-induced reflection changes from a gold grating measured with a 400 nm central wavelength probe beam for different excitation fluences and for pump wavelengths below (640 nm), at (650 nm), and above (660 nm) the SPP resonance.

orthogonal to the grating lines. We illuminate the sample using three different pump wavelengths of 640, 650, and 660 nm, which are below, on, and above the SPP resonance wavelength, respectively. At t = 0, we measure a pulse-length-limited decrease in reflection directly after excitation, governed by electron dynamics.[33,34] Afterward, the electrons will cool to the lattice via the emission of phonons. This results in rapid heating of the layer, which causes a thermal stress to form. The growth of the thermal stress then launches a strain wave.[2] Due to the geometry of the sample, multiple types of acoustic waves are launched, each having its own frequency. These different types of acoustic waves are described in more detail elsewhere.[31] Briefly, we identified a longitudinal wave (LW), a surface acoustic wave (SAW), and a grating-line-normal mode (NM). These different types of strain waves result in both relatively low- and high-frequency time-dependent reflection changes.

We measure remarkably strong strain-wave-induced reflection changes, with a magnitude of ~0.7% for the highest pump fluences used in our experiments. The signal is strongest when the pump beam is exactly tuned to the SPP resonance and becomes smaller when the pump is tuned to wavelengths above or below the resonance. This is consistent with the fact that when the wavelength is tuned to the resonance, the absorption is strongest, leading to a stronger strain wave. As mentioned before, we launch multiple types of acoustic waves, each with its own frequency. We can determine the strain-induced signal strength for each frequency from the fast Fourier transform (FFT) of the time-dependent data. From the FFT, we extract four prominent frequencies, located at 2.8 GHz (SAW), 7.0 GHz (NM), 10.0 GHz (unknown), and 12.3 GHz (LW). In Fig. 3, we show the magnitude of these four most prominent frequencies as a function of pump fluence for all pump wavelengths. Surprisingly,

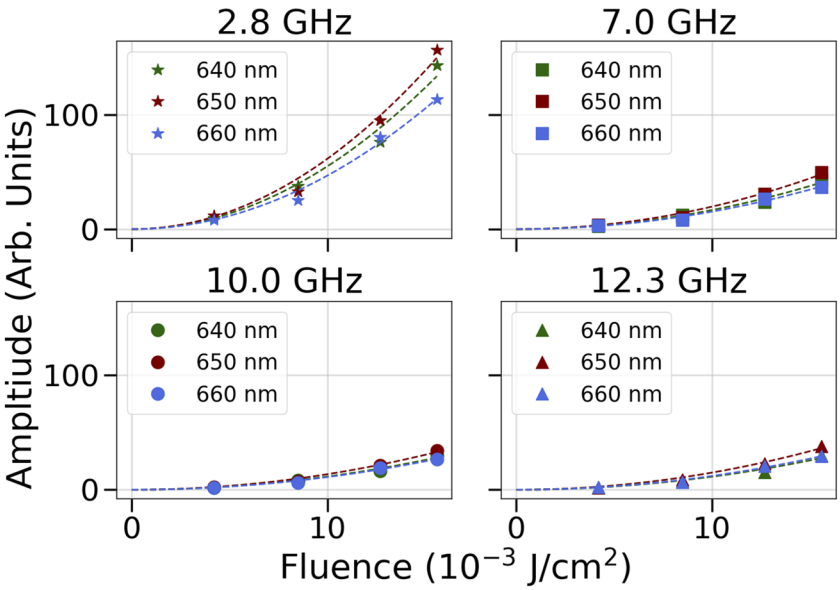

FIG. 3. FFT amplitudes of the four most prominent frequencies as a function of incident pump fluence for three different pump wavelengths. The dashed lines, going through the data points, represent quadratic fits to the data. The agreement between the data and the fit indicates that the amplitude of the strain-induced reflection changes scales non-linearly with the incident pump fluence for all measured frequencies.

we notice an approximately quadratic increase of the strain-induced reflection changes for all measured frequencies.

To better understand the observed non-linear behavior of the signal strength vs pump power, we first have to determine whether the non-linearity occurs in the generation process or in the detection process. A non-linear response in the generation of the strain wave could be the result of the non-linear absorption of the pump beam by, for example, two-photon absorption.[35] However, by measuring the absorption of the gold grating as a function of incident power, we find that, within our measurement accuracy of ~1%, the absorbed pump energy scales linearly with the incident pump energy for all pump fluences up to the highest pump fluence used in the experiments of 15.6×10^{-3} J/cm^2. Independent of the incident pump fluence, ~65% of the pump energy is absorbed. Note that this is much more than what is typically absorbed by a flat gold surface at a wavelength of 650 nm and shows the enhanced absorption caused by the SPP resonance.

Another potential non-linear effect in the generation process is that the magnitude of the generated strain might scale non-linearly with the absorbed pump power. A frequently used model by Thomsen *et al.*,[36] which we have used in the past to describe the generation and propagation of strain waves,[32] cannot be used here because it assumes that the strain scales linearly with the amount of absorbed energy. In order to identify if the strain itself scales non-linearly with the absorbed pump-power, we have performed the same pump–probe experiments with the roles of pump and probe reversed. A different sample with a somewhat thinner, 117 nm gold layer, but with the same period and amplitude, was used in this case as the original one was destroyed in another experiment. We excited the gold grating with a pump wavelength of 400 nm and measured the strain-wave-induced reflection changes at a wavelength of 660 nm and also at 640 nm (not shown here). The SPP resonance is still fixed at 650 nm. We note that, to determine whether the strain scales non-linearly with absorbed power, we have to ensure that we cover the same range of absorbed energies as before. For the grating with the 117 nm thick gold layer, we measure an absorption of some 79 percent at the 400 nm pump wavelength. This should be compared to the value of 65 percent measured when pumping at the plasmonic wavelength of 650 nm. Considering the ranges of fluences used in both experiments, we can conclude that the ranges of absorbed pump energies are similar in both experiments.

In Fig. 4, we show the time dependent pump-induced reflection changes (left graph) and the fluence-dependent magnitudes (right graph) of three different acoustic modes at a probe wavelength of 660 nm, measured for this sample. One immediately notices the relatively strong quasi static thermal background in the measurements, which is much less dominant when pumping at 650 nm and probing at 400 nm. The acoustic oscillations seen superimposed on this background have a similar amplitude as the one shown in Fig. 2 but have a somewhat different shape.

Here also, an FFT analysis shows that multiple acoustic modes are launched in our experiments. The ones we have been able to identify are the SAW (2.6 GHz) and the NM (6.8 GHz), which have similar frequencies to the one we have observed for the grating covered with 139 nm Au. There is also a mode at 13.8 GHz that corresponds to the frequency of the LM mode for a gold layer thickness of 117 nm. The other modes that we have not been able to identify yet and are not shown here, but they show a similar fluence dependence. The dashed lines in the figure on the right are linear fits to the data points. They strongly suggest that the measured acoustic mode amplitudes vs fluence show a close-to-linear dependence as opposed to the quadratic dependence seen when pumping around 650 nm wavelengths and probing at a 400 nm wavelength.

We emphasize again that the ranges of absorbed pump energies are comparable in both experiments. Our results, therefore, suggest that the non-linear relation between the magnitude of the reflection changes and the absorbed pump energy that we observe in Fig. 3 may be caused by a wavelength dependence in the strain wave *detection*.

It has been shown that strain can directly change the band-structure of materials,[37–41] even in such a manner that strain can induce semiconductor-to-metal transitions.[42–45] Furthermore, it has been demonstrated that strain can increase or decrease the bandgap and interband transition energy of materials,[46–51] also in a non-linear manner.[52] For gold, in particular, the interband transition from the d-band to the hybridized s/p-band is very sensitive to strain.[53,54] In our experiments, the probe wavelength equals 400 nm, and thus we excite electrons from the d-band to the hybridized s/p-band.[34] We speculate that the strong non-linear reflectivity changes vs pump power are due to strain-induced changes in the interband transition energy.

We can estimate how much the interband transition energy in gold has to change to reproduce the magnitude of our measured reflection changes, using a dielectric function that takes into account interband transitions from the d-band to the hybridized s/p-band. This function is given by[55–58]

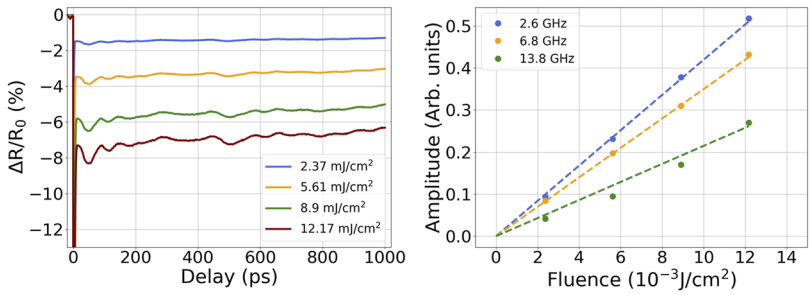

FIG. 4. The left pane shows the pump-induced reflection changes from a gold grating measured with a 660 nm central wavelength probe beam for different excitation fluences, the pump wavelength equals 400 nm. The right pane shows the FFT magnitudes for the measured acoustic frequencies as a function of incident pump fluence.

$$\varepsilon(\omega) = \underbrace{\varepsilon_\infty - \frac{\omega_p^2}{\omega\left(\omega + \frac{i}{\tau_c}\right)}}_{\varepsilon_{intra}} \underbrace{- \frac{4\pi e^2}{m^2\omega^2} \sum_{\mathbf{k}\mathbf{k}'bb'} \frac{\left(\hbar\omega + \frac{i}{\tau_{bb'}}\right)\langle b\mathbf{k}|p_i|b'\mathbf{k}'\rangle\langle b'\mathbf{k}'|p_i|b\mathbf{k}\rangle}{(E_{b'k'} - E_{bk})\left(E_{b'k'} - E_{bk} - \hbar\omega - \frac{i}{\tau_{bb'}}\right)}(f_0(E_{b'k'}) - f_0(E_bk))}_{\varepsilon_{inter}}, \quad (1)$$

where ε is the frequency-dependent permittivity, consisting of two terms ε_{intra} and ε_{inter}, which describe the contributions by intraband and interband transitions to the permittivity, respectively. ε_∞ is a constant contribution to the dielectric function due to all other bound transitions, ω_p is the plasma frequency, e is the electronic charge, m is the effective electron mass, $\hbar$ is the reduced Planck's constant, $\mathbf{k}$ is the momentum of an electron in band b, τ_c is the inverse intraband damping rate, τ_{bb} is the interband equivalent of τ_c, $\langle b\mathbf{k}|p_i|b'\mathbf{k}'\rangle\langle b'\mathbf{k}'|p_i|b\mathbf{k}\rangle$ is the transition matrix element, E_{bk} is the energy of an electron in band b with momentum $\mathbf{k}$, and f_0 is the Fermi distribution.

For gold, we can approximately describe the d-band as a completely filled flat band and the s/p-band as a half-filled parabolic band. The momentum-dependent energy of the bands is approximated by[56]

$$E_{d,k} = 0, \quad (2)$$

$$E_{s/p,k} = \frac{\hbar^2 k^2}{2m} + \Delta, \quad (3)$$

where Δ is the interband transition energy. If we plug Eqs. (2) and (3) into Eq. (1), we end up with a dielectric function that depends on the interband transition energy. We then calculate the reflection from the dielectric function.

In Fig. 5(a), we show the calculated $\Delta R/R$ as a function of Δ. In the regime of the reflection changes measured in our experiments, we find that the reflection changes scale linearly with Δ. In Fig. 5(b), we show the maximum interband transition energy Δ_{max} required to account for the measured maximum reflection changes, vs the pump fluence. We find that the maximum strain-induced change of the interband transition energy needed to obtain the highest measured reflection change is ~0.013 eV. Since the strain scales linearly with the incident power and the reflection changes scale linearly with Δ, we conclude that Δ would have to scale approximately quadratically with the strain to explain our data. We caution that the model we used here assumes that the strain only affects Δ. In reality, it seems likely that the strain also influences the shape of the band structure itself. Nevertheless, the calculation gives an order-of-magnitude estimate of the required maximum change in Δ and implies that this would require a roughly quadratic relation between the strain and Δ, which is not unreasonable to assume.[52,53]

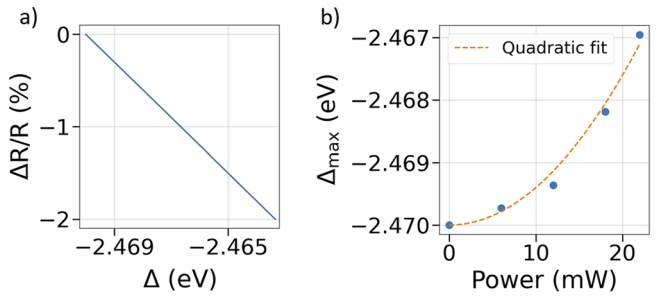

FIG. 5. (a) Calculated change in reflectivity as a function of interband transition energy. (b) Calculated required maximum change of the interband transition energy, Δ_{max}, induced by the longitudinal strain needed to retrieve the magnitude of our measured reflection changes. We see that Δ_{max} has to change by only 0.013 eV to account for the measured reflection changes. The dashed line is a quadratic fit to the data and serves as a guide to the eye.

B. Diffraction

In Fig. 6(a), we show a measurement of the time-dependent diffraction change and the time-dependent reflection change in the same plot. The pump wavelength equals 650 nm, and the pump fluence equals 15.6×10^{-3} J/cm^2. Note that here, in contrast to transient-grating measurements,[3,32] we measure a 0.7% modulation of the diffraction efficiency on top of a static background diffraction from the fixed, physical grating. Even though the excitation is identical for both the reflection and diffraction measurements, the shape of the time-dependent response is different. For both reflection and diffraction, we measure a pulse-length-limited signal decrease caused by electron dynamics, with a rapid recovery within ~5 ps. Afterward, both the diffraction and reflection start to slowly

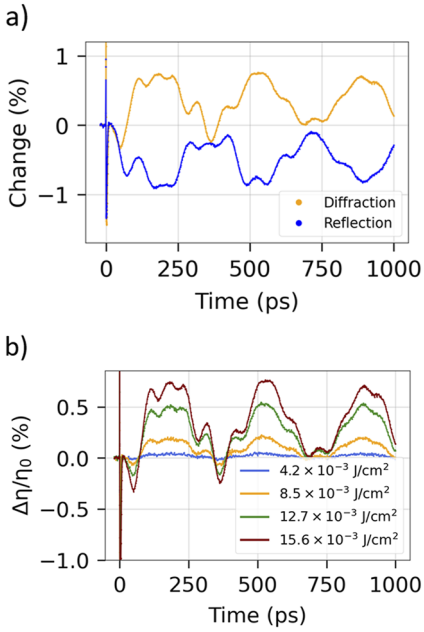

FIG. 6. (a) Measured pump induced diffraction and reflection change of the 400 nm probe pulse from the gold grating. (b) Pump-power-dependent measurement of the strain-wave-induced diffraction changes.

decrease. After ~50 ps, the diffraction change starts to increase, while the reflection starts to decrease further. From here on, reflection and diffraction behave differently.

For both diffraction and reflection, we measure a slow oscillation with a frequency of 2.8 GHz. However, this frequency induces diffraction and reflection changes that are opposite in sign. Compared to the reflection measurements, the higher frequency oscillations in the diffraction measurement seem to have shifted slightly from 10.0 to 9.5 GHz and from 12.0 to 12.7 GHz. Furthermore, the 7.0 GHz frequency, which is present in the reflection spectrum, is no longer present in the diffraction measurement. The cause of these small changes in the apparent position of the peaks as measured in diffraction is currently not well understood. Other, more subtle, discrepancies in the temporal response of the diffraction and reflection to the *same* strain wave are attributed to the fact that reflection is *only* sensitive to the strain-optic effect, while diffraction is sensitive to *both* the strain-optic effect *and* strain-induced deformation and displacement of the grating lines.

In Fig. 6(b), we show the pump power dependence of the strain-wave-induced diffraction changes. Similar to the pump power-dependent reflection measurements, as shown in Fig. 2, we measure a roughly quadratic dependence of the strain wave-induced diffraction efficiency as a function of pump power. Intuitively, one would expect that the diffraction efficiency would scale quadratically with the incident power because the diffraction efficiency of a square grating scales quadratically with the grating amplitude.[59] However, this is only true in a background-free measurement, i.e., when no static background diffraction is present. This is *not* the case in our measurements since we have a static background diffraction of 11%. It has been shown that, when a strong background field is present, such a quadratic dependence reduces to a linear dependence when the background field is much stronger than the strain-induced diffracted field, which is the case here.[26] Despite this, we still measure a quadratic dependence of the diffraction efficiency on the pump power and attribute this to the same nonlinear change in the interband transition energy as for the reflection measurements.

IV. CONCLUSION

In summary, we have shown efficient excitation of ultrasonic strain waves on a gold grating by using surface plasmon polaritons to enhance the coupling of the light to the grating. We measure strong time-dependent strain-wave-induced reflection and diffraction changes on the order of 0.7%. Furthermore, we have shown that the amplitude of the measured reflection changes scales non-linearly with the fluence of the pump beam for a probe wavelength of 400 nm. We argue that this non-linear behavior is possibly linked with non-linear changes of the interband transition energy as a function of strain. In order to account for the amplitude of the measured reflection changes, the interband transition energy would need to decrease by 0.013 eV.

ACKNOWLEDGMENTS

The authors would like to thank the Universiteit van Amsterdam, ASML, and the Nederlandse Organisatie voor Wetenschappelijk Onderzoek for funding this research.

AUTHOR DECLARATIONS

Conflict of Interest

The authors have no conflicts to disclose.

DATA AVAILABILITY

The data that support the findings of this study are available from the corresponding author upon reasonable request.

REFERENCES

[1] J. Wang and C. Guo, "Effect of electron heating on femtosecond laser-induced coherent acoustic phonons in noble metals," Phys. Rev. B **75**, 184304 (2007).
[2] P. Ruello and V. E. Gusev, "Physical mechanisms of coherent acoustic phonons generation by ultrafast laser action," Ultrasonics **56**, 21–35 (2015).
[3] H. Zhang, A. Antoncecchi, S. Edward, I. Setija, P. Planken, and S. Witte, "Unraveling phononic, optoacoustic, and mechanical properties of metals with light-driven hypersound," Phys. Rev. Appl. **13**, 014010 (2020).
[4] T. Saito, O. Matsuda, and O. B. Wright, "Picosecond acoustic phonon pulse generation in nickel and chromium," Phys. Rev. B **67**, 205421 (2003).
[5] J. L. Arlein, S. E. Palaich, B. C. Daly, P. Subramonium, and G. A. Antonelli, "Optical pump-probe measurements of sound velocity and thermal conductivity of hydrogenated amorphous carbon films," J. Appl. Phys. **104**, 033508 (2008).
[6] G. Tas and H. J. Maris, "Electron diffusion in metals studied by picosecond ultrasonics," Phys. Rev. B **49**, 15046–15054 (1994).
[7] V. E. Gusev and O. B. Wright, "Ultrafast nonequilibrium dynamics of electrons in metals," Phys. Rev. B **57**, 2878–2888 (1998).
[8] O. B. Wright and K. Kawashima, "Coherent phonon detection from ultrafast surface vibrations," Phys. Rev. Lett. **69**, 1668–1671 (1992).
[9] A. Devos and C. Lerouge, "Evidence of laser-wavelength effect in picosecond ultrasonics: Possible connection with interband transitions," Phys. Rev. Lett. **86**, 2669–2672 (2001).
[10] A. Devos, R. Cote, G. Caruyer, and A. Lefvre, "A different way of performing picosecond ultrasonic measurements in thin transparent films based on laser-wavelength effects," Appl. Phys. Lett. **86**, 211903 (2005).
[11] D. Schneider, T. Witke, T. Schwarz, B. Schoneich, and B. Schultrich, "Testing ultra-thin films by laser-acoustics," Surf. Coat. Technol. **126**, 136–141 (2000).
[12] H. T. Grahn, H. J. Maris, J. Tauc, and B. Abeles, "Time-resolved study of vibrations of a-Ge:H/a-Si:H multilayers," Phys. Rev. B **38**, 6066 (1988).
[13] A. Haim, S. Bar-Ad, and A. Azoulay, "Elastic characterization of Au thin films utilizing laser induced acoustic Rayleigh waves," J. Phys.: Conf. Ser. **278**, 012005 (2011).
[14] B. Perrin, B. Bonello, J.-C. Jeannet, and E. Romatet, "Picosecond ultrasonics study of metallic multilayers," Physica B **219–220**, 681–683 (1996).
[15] A. Devos and A. Le Louarn, "Strong effect of interband transitions in the picosecond ultrasonics response of metallic thin films," Phys. Rev. B **68**, 045405 (2003).
[16] A. Devos and R. Cote, "Strong oscillations detected by picosecond ultrasonics in silicon: Evidence for an electronic-structure effect," Phys. Rev. B **70**, 125208 (2004).
[17] R. I. Tobey, E. H. Gershgoren, M. E. Siemens, M. M. Murnane, H. C. Kapteyn, T. Feurer, and K. A. Nelson, "Nanoscale photothermal and photoacoustic transients probed with extreme ultraviolet radiation," Appl. Phys. Lett. **85**, 564–566 (2004).
[18] R. I. Tobey, M. E. Siemens, M. M. Murnane, H. C. Kapteyn, D. H. Torchinsky, and K. A. Nelson, "Transient grating measurement of surface acoustic waves in thin metal films with extreme ultraviolet radiation," Appl. Phys. Lett. **89**, 091108 (2006).
[19] G. A. Antonelli, P. Zannitto, and H. J. Maris, "New method for the generation of surface acoustic waves of high frequency," Physica B **316–317**, 377–379 (2002).
[20] T. Saito, O. Matsuda, M. Tomoda, and O. B. Wright, "Imaging gigahertz surface acoustic waves through the photoelastic effect," J. Opt. Soc. Am. B **27**, 2632 (2010).
[21] M. R. Armstrong, E. J. Reed, K. Y. Kim, J. H. Glownia, W. M. Howard, E. L. Piner, and J. C. Roberts, "Observation of terahertz radiation coherently generated by acoustic waves," Nat. Phys. **5**, 285–288 (2009).

[22]R. M. Slayton, K. A. Nelson, and A. A. Maznev, "Transient grating measurements of film thickness in multilayer metal films," J. Appl. Phys. **90**, 4392–4402 (2001).
[23]S. Edward, H. Zhang, I. Setija, V. Verrina, A. Antoncecchi, S. Witte, and P. C. M. Planken, "Detection of hidden gratings through multilayer nanostructures using light and sound," Phys. Rev. Appl. **10**, 014015 (2019); arXiv:1911.08337.
[24]S. Edward, H. Zhang, S. Witte, and P. C. M. Planken, "Laser-induced ultrasonics for detection of low-amplitude grating through metal layers with finite roughness," Opt. Express **28**, 23374 (2020).
[25]S. Edward, H. Zhang, I. Setija, V. Verrina, A. Antoncecchi, S. Witte, and P. C. M. Planken, "Detection of hidden gratings through multilayer nanostructures using light and sound," Phys. Rev. Appl. **14**, 014015 (2020).
[26]V. Verrina, S. Edward, H. Zhang, S. Witte, and P. C. M. Planken, "Photoacoustic detection of low duty cycle gratings through optically opaque layers," Appl. Phys. Lett. **117**, 051104 (2020).
[27]V. Verrina, S. Edward, H. Zhang, A. Antoncecchi, S. Witte, and P. C. M. Planken, "Role of scattering by surface roughness in the photoacoustic detection of hidden micro-structures," Appl. Opt. **59**, 9499 (2020).
[28]A. Antoncecchi, H. Zhang, S. Edward, V. Verrina, P. C. M. Planken, and S. Witte, "High-resolution microscopy through optically opaque media using ultrafast photoacoustics," Opt. Express **28**, 33937 (2020).
[29]B. C. Daly, N. C. Holme, T. Buma, C. Branciard, T. B. Norris, D. M. Tennant, J. A. Taylor, J. E. Bower, and S. Pau, "Imaging nanostructures with coherent phonon pulses," Appl. Phys. Lett. **84**, 5180–5182 (2004).
[30]T. F. Crimmins, A. A. Maznev, and K. A. Nelson, "Transient grating measurements of picosecond acoustic pulses in metal films," Appl. Phys. Lett. **74**, 1344–1346 (1999).
[31]G. de Haan, V. Verrina, A. J. L. Adam, H. Zhang, and P. C. M. Planken, "Plasmonic enhancement of photoacoustic-induced reflection changes," Appl. Opt. **60**, 7304–7313 (2021).
[32]G. de Haan, T. J. van den Hooven, and P. C. M. Planken, "Ultrafast laser-induced strain waves in thin ruthenium layers," Opt. Express **29**, 32051 (2021).
[33]S. Edward, A. Antoncecchi, H. Zhang, H. Sielcken, S. Witte, and P. C. M. Planken, "Detection of periodic structures through opaque metal layers by optical measurements of ultrafast electron dynamics," Opt. Express **26**, 23380–23396 (2018).
[34]J. Hohlfeld, S.-S. Wellershoff, J. Güdde, U. Conrad, V. Jähnke, and E. Matthias, "Electron and lattice dynamics following optical excitation of metals," Chem. Phys. **251**, 237–258 (2000).
[35]M. Rumi and J. W. Perry, "Two-photon absorption: An overview of measurements and principles," Adv. Opt. Photonics **2**, 451 (2010).
[36]C. Thomsen, H. T. Grahn, H. J. Maris, and J. Tauc, "Surface generation and detection of phonons by picosecond light pulses," Phys. Rev. B **34**, 4129–4138 (1986).
[37]P. D. Khang, M. Davoudiniya, L. T. T. Phuong, T. C. Phong, and M. Yarmohammadi, "Optical interband transitions in strained phosphorene," Phys. Chem. Chem. Phys. **21**, 15133–15141 (2019).
[38]M. Ghorbani-Asl, S. Borini, A. Kuc, and T. Heine, "Strain-dependent modulation of conductivity in single-layer transition-metal dichalcogenides," Phys. Rev. B **87**, 235434 (2013); arXiv:1301.3469.
[39]W. S. Yun, S. W. Han, S. C. Hong, I. G. Kim, and J. D. Lee, "Thickness and strain effects on electronic structures of transition metal dichalcogenides: 2H-*MX*2 semiconductors (*M* = Mo, W; *X* = S, Se, Te)," Phys. Rev. B **85**, 033305 (2012).
[40]P. Lu, X. Wu, W. Guo, and X. C. Zeng, "Strain-dependent electronic and magnetic properties of MoS_2 monolayer, bilayer, nanoribbons and nanotubes," Phys. Chem. Chem. Phys. **14**, 13035–13040 (2012).
[41]H. Peelaers and C. G. Van De Walle, "Effects of strain on band structure and effective masses in MoS_2," Phys. Rev. B **86**, 241401(R) (2012).
[42]E. Scalise, M. Houssa, G. Pourtois, V. Afanas'ev, and A. Stesmans, "Strain-induced semiconductor to metal transition in the two-dimensional honeycomb structure of MoS_2," Nano Res. **5**, 43–48 (2012).
[43]S. Bhattacharyya and A. K. Singh, "Semiconductor-metal transition in semiconducting bilayer sheets of transition-metal dichalcogenides," Phys. Rev. B **86**, 075454 (2012); arXiv:1203.6820.
[44]A. Kumar and P. K. Ahluwalia, "Semiconductor to metal transition in bilayer transition metals dichalcogenides MX_2 (M = Mo, W; X = S, Se, Te)," Modell. Simul. Mater. Sci. Eng. **21**, 065015 (2013).
[45]A. P. Nayak, S. Bhattacharyya, J. Zhu, J. Liu, X. Wu, T. Pandey, C. Jin, A. K. Singh, D. Akinwande, and J. F. Lin, "Pressure-induced semiconducting to metallic transition in multilayered molybdenum disulphide," Nat. Commun. **5**, 3731 (2014).
[46]A. Visibile, R. B. Wang, A. Vertova, S. Rondinini, A. Minguzzi, E. Ahlberg, and M. Busch, "Influence of strain on the band gap of Cu_2O," Chem. Mater. **31**, 4787–4792 (2019).
[47]X. Dou, K. Ding, D. Jiang, and B. Sun, "Tuning and identification of interband transitions in monolayer and bilayer molybdenum disulfide using hydrostatic pressure," ACS Nano **8**, 7458–7464 (2014).
[48]A. Ramasubramaniam, D. Naveh, and E. Towe, "Tunable band gaps in bilayer transition-metal dichalcogenides," Phys. Rev. B **84**, 205325 (2011).
[49]K. He, C. Poole, K. F. Mak, and J. Shan, "Experimental demonstration of continuous electronic structure tuning via strain in atomically thin MoS_2," Nano Lett. **13**, 2931–2936 (2013).
[50]H. J. Conley, B. Wang, J. I. Ziegler, R. F. Haglund, S. T. Pantelides, and K. I. Bolotin, "Bandgap engineering of strained monolayer and bilayer MoS_2," Nano Lett. **13**, 3626–3630 (2013); arXiv:1305.3880.
[51]C. R. Zhu, G. Wang, B. L. Liu, X. Marie, X. F. Qiao, X. Zhang, X. X. Wu, H. Fan, P. H. Tan, T. Amand, and B. Urbaszek, "Strain tuning of optical emission energy and polarization in monolayer and bilayer MoS_2," Phys. Rev. B **88**, 121301(R) (2013); arXiv:1306.3442.
[52]K. Guilloy, N. Pauc, A. Gassenq, Y.-M. Niquet, J.-M. Escalante, I. Duchemin, S. Tardif, G. Osvaldo Dias, D. Rouchon, J. Widiez, J.-M. Hartmann, R. Geiger, T. Zabel, H. Sigg, J. Faist, A. Chelnokov, V. Reboud, and V. Calvo, "Germanium under high tensile stress: Nonlinear dependence of direct band gap vs strain," ACS Photonics **3**, 1907–1911 (2016); arXiv:1606.01668.
[53]N. Egede Christensen and B. O. Seraphin, "Relativistic band calculation and the optical properties of gold," Phys. Rev. B **4**, 3321–3344 (1971).
[54]P. Szczepanek and R. Glosser, "Piezo-optical constants of gold," Solid State Commun. **15**, 1425–1429 (1974).
[55]K. C. Rustagi, "Bilinear optical polarizability of silver," Nuovo Cimento B **53**, 346–362 (1968).
[56]J. Hohlfeld, D. Grosenick, U. Conrad, and E. Matthias, "Femtosecond time-resolved reflection second-harmonic generation on polycrystalline copper," Appl. Phys. A **60**, 137–142 (1995).
[57]S. S. Jha and C. S. Warke, "Interband contributions to optical harmonic generation at a metal surface," Phys. Rev. **153**, 751–759 (1967).
[58]J. Hohlfeld, U. Conrad, J. G. Müller, S.-S. Wellershoff, E. Matthias, and K. H. Bennemann, *Nonlinear Optics in Metals* (Oxford University, 1998), pp. 219–267.
[59]Y. C. Chang, P. Zhou, and J. H. Burge, "Analysis of phase sensitivity for binary computer-generated holograms," Appl. Opt. **45**, 4223–4234 (2006).